Rare Met. (2022) 41(10):3560–3565
https://doi.org/10.1007/s12598-016-0723-6

RARE METALS
www.editorialmanager.com/rmet

Microstructural refinement and performance improvement of Cu–36 wt% Zn alloy by Al_2O_3 nanoparticles coupling electromagnetic stirring

Ya-Bo Fu*, Yi-Ping Lu, Zhi-Jun Wang, Zhi-Qiang Cao, Ai-Jiao Xu

Received: 28 January 2015 / Revised: 27 March 2015 / Accepted: 29 March 2016 / Published online: 28 April 2016

Abstract Cu–36 wt% Zn alloy is widely used in valves of water and heating and auto parts, etc. Nevertheless, the structure is still coarse, and performances are much poor. The structure and performances of Cu–36 wt% Zn alloy were investigated by adding Al_2O_3 nanoparticles and stirring. Results indicate that by Al_2O_3 nanoparticles coupling electromagnetic stirring, the Cu–36 wt% Zn alloy with refined microstructure was successfully prepared. The average grain size is refined by 99 % compared with that without nanoparticles and stirring. The tensile strength (R_m) and percentage elongation after fracture ($A_{11.3}$) increase by 20.58 % and 19.40 %, respectively, compared with that without nanoparticles and stirring. Nanoparticles increase heterogeneous nucleation rate by 50 % compared with that without nanoparticles. The depth of dezincification layer decreases by 78.71 % compared with that without nanoparticles and stirring, as protective layer (Cu–Al_2O_3–Zn) is completely formed around the grain boundaries.

Keywords Microstructural refinement; Rotating electromagnetic field; Mechanical performance; Al_2O_3 nanoparticles

Y.-B. Fu*, A.-J. Xu
School of Physics and Electronic Engineering, Taizhou University, Taizhou 318000, China
e-mail: Lgdfyb@163.com

Y.-P. Lu, Z.-Q. Cao
School of Materials Science and Engineering, Dalian University of Technology, Dalian 116024, China
e-mail: luyiping@dlut.edu.cn

Z.-J. Wang
School of Materials Science and Engineering, Northwestern Polytechnical University, Xi'an 710048, China

1 Introduction

Cu–36 wt% Zn alloy (C46500 of American brand) is widely used in valves of water and heating and auto parts, etc., due to its excellent mechanical property, process performance, and corrosion resistance [1]. However, the solidification structures in casting generally produce coarse grains which lead to fracture in machining process. Corrosion resistance is also an important performance; however, in seawater and air with O_2, CO_2, H_2S, NH_3, the corrosion rate increases. Kobayashi [2] and Zhang and Xu [3] have found that Ti and B can refine the structure of Cu–Zn alloy, and 0.0001 wt%–0.0010 wt% B can transform columnar crystals to equiaxial crystals of 30–50 μm. Ni can enhance the dezincification corrosion and stress corrosion owing to expanding α phase area [4]. 0.02 wt%–0.06 wt% As can also inhibit dezincification by hindering the zinc preferent dissolution as the protective layer (Cu–As–Zn) was completely formed around the grain boundaries [5]. By adding B and As, the depth of dezincification layer was 131–187 μm after the heat treatment of extrusion billet with 480 °C for 6 h [6]. However, the structure is still coarse, and performances are much poor. Especially equiaxial grain of less than 30–50 μm in size and dezincification layer of less than 131 μm in depth are not reported for brass. So many researchers pay attention to refining the structure and improving the performances of Cu–Zn alloy.

Electromagnetic processing of materials (EPM) has been widely applied in the improvement of solidification structure and mechanical properties of materials by controlling their solidification behaviors [7]. Over the past two decades, much work has been done to control the solidification process and structure by pulsed physical fields, such as pulsed magnetic field [8–10], its oscillation [11], and

electric current pulse (ECP). [12–14]. Rodriguez et al. [15] used alternating magnetic field of commercial frequency to horizontal continuous casting of copper tubes, whose solidification structure was substantially refined. Li et al. [16] and Yan et al. [17] applied commercial frequency to copper alloy tubes and obtained prominent progress. Song et al. [18] studied the method of internal oxidation to produce the copper-based composite with high strength and found Al_2O_3 particles with diameter of 10–30 nm were evenly distributed in the copper matrix. In recent years, more and more attention has been focused on nanoparticles addition to improve the solidification structure and mechanical properties of composite. Chen et al. [19] studied the corrosion resistance of casting austenitic stainless steel added with nanoparticles and also studied the solidification structure refinement and properties of Cu–Zn–Al alloy modified by SiC nanoparticles, resulting in refined solidification structure and enhanced properties. In our view, Cu–36 wt% Zn alloy is becoming a promising material, so it is necessary to improve the properties of Cu–36 wt% Zn alloy by stirring and adding Al_2O_3 nanoparticles.

In this paper, Cu–36 wt% Zn alloy with refined structure was prepared by horizontal electromagnetic continuous casting and adding Al_2O_3 nanoparticles which was modified. And then the performances of low depth of dezincification layer, tensile strength, percentage elongation after fracture, and dezincification corrosion resistance were studied.

2 Experimental

Experimental setup consists of a holding furnace, withdrawal system, water-cooling system, stirrer system, graphite inner mold, and a melting furnace. Figure 1 shows a schematic diagram of the experimental setup with a melting furnace. The water-cooling system was composed of copper outer jacket and stainless steel cover. The diameter of graphite inner mold is 90 mm for four billets, the taper of inner mold is 1°, and the diameter of billets is 16 mm. The nominal composition of Cu–36 wt% Zn alloy as the studied material is Cu 61.000 wt%–63.000 wt%, Zn 35.000 wt%–37.000 wt%, Sn 0.600 wt%–1.000 wt%, Fe 0.080 wt%–1.000 wt%, Si 0.100 wt%–0.200 wt%, B 0.006 wt%–0.008 wt%. Commercial Al_2O_3 nanoparticles are one-dimensional nanomaterial with diameter of 40–80 nm and length of 200–500 nm and were modified with dispersing agent NET401 and graining by planetary ball milling for 3 h at 300 r·min^{-1}. Before put in the intermediate frequency melting furnace, about 10 g powder mixture was inserted in

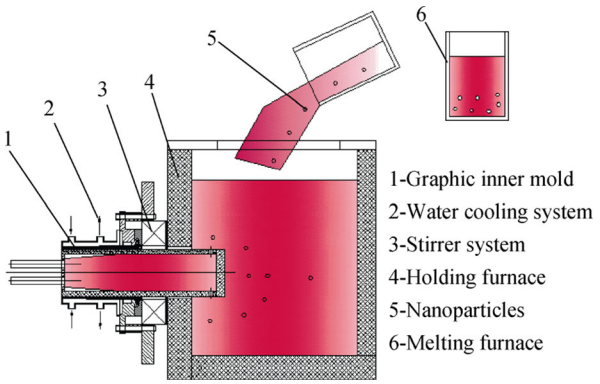

Fig. 1 Schematic diagram of experimental setup with a melting furnace

an iron foil to form a packet of composite as reinforcement. Modified Al_2O_3 nanoparticles (0.10 wt% of total liquid metals) and nominal composition of Cu–36 wt% Zn alloy were molten and superheated to 1093 °C. After holding and manual stirring for 60 min, the molten metal was poured into holding furnace holding for 30 min. Then, the bar with a diameter of 16 mm was continuously cast with rotating electromagnetic field (REM) at 50 A and 30 Hz. The macrostructure in Fig. 2 was etched by 50 vol% HNO_3 and 50 vol% water. The samples were etched by solution mixed with 3 g $FeCl_3$, 2 ml HCl, and 96 ml C_2H_5OH for 1–2 min and then studied by scanning electron microscope (SEM, S4800) and optical microscope (OM, Zeiss Axio Scope A1) to observe the microstructure. The average grain size was measured by inverted metallurgical microscope (Model GX71) and was calculated with 50 grains by five times through following equation:

$$d = \frac{L}{MN} \tag{1}$$

where d is the grain size, L is the total length of cutting line, N is the magnification times, and M is the number of cutoff point with grain boundary through L.

Specimens of dezincification corrosion with the cube (length of 10 mm, width of 10 mm, and height of 10 mm) were immersed in a glass container containing 10 g·L^{-1} $CuCl_2$ solution for 24 h at steady temperature of 75 °C. Experiments of electrochemical corrosion were performed with an electrochemical workstation of CHI600. Traditional three electrodes of a specimen, a platinum electrode, and a saturated calomel electrode (SCE) were used as a working electrode, a counter electrode, and a reference electrode, respectively. Curves of potentiodynamic polarization were obtained after 10-min immersion in 3.2 wt% NaCl solution at a scan rate of 1 mV·s^{-1}. Tensile strength, percentage elongation after fracture, and dezincification

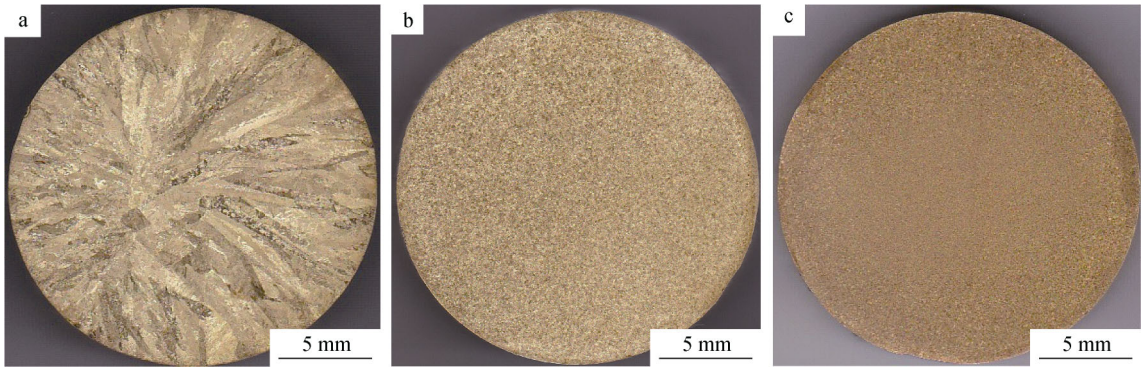

Fig. 2 Macrostructures of Cu–36 wt% Zn alloy: **a** without REM and nanoparticles, **b** with REM, and **c** with REM coupling Al_2O_3 nanoparticles

corrosion resistance were studied by universal testing machine (SANS CMT5305), SEM, and OM.

3 Results and discussion

3.1 Study of refined structure

3.1.1 Effect of Al_2O_3 nanoparticles on structure

Figure 2a shows the macrostructure of Cu–36 wt% Zn (matrix alloy) without REM and nanoparticles. The solidification structure is coarse when the average grain size is about 1.7 mm. Figure 2b shows the structure with REM, which is much finer than that in Fig. 2a (0.034 mm in average grain size). Figure 2c shows the structure with REM coupling Al_2O_3 nanoparticles. The average grain size is about 0.017 mm, which decreases by 99 % compared with that without nanoparticles and stirring. In order to maintain uniform casting conditions, the same casting parameters were applied to all samples as below: drawing speed of 360 mm·min^{-1}, flow rate of cooling water of 2.776 m^3·h^{-1}, and holding in furnace at 1093 °C for 30 min for the uniformity of composition and temperature. For the third sample, modified nanoparticles were added into the melting furnace and held for 60 min to make nanoparticles disperse, and then, the molten metal of composite was poured into the furnace held for 30 min to start casting. At the same time, REM was applied to stirring the liquid during casting, and the average grain size is about 0.017 mm. The result shows that the average grain size of Cu–36 wt% Zn alloy by adding Al_2O_3 nanoparticles is the most refined in the three specimens.

3.1.2 Mechanism of refined structures

Generally, a liquid at the temperature either above or below its melting point will have a distribution of solid-like clusters [20, 21]. According to the classical heterogeneous nucleation theory [22, 23], the heterogeneous nucleation rate (I) can be given by [24]:

$$I = I_0 \exp\left(-\frac{\Delta G_{\mathrm{d}}}{kT}\right) \exp\left(-\frac{\Delta G_{\mathrm{V}}}{kT} f(\theta)\right) \tag{2}$$

$$I = N_n^0 \frac{\mathrm{d}n}{\mathrm{d}t} \tag{3}$$

where I_0 and k are constants, ΔG_{d} is the diffusion activation energy, ΔG_{V} is the Gibbs free energy of liquid and solid, T is the melting temperature, $f(\theta)$ is the function of wetting angle, N_n^0 is the number of crystals with critical size, and $\frac{\mathrm{d}n}{\mathrm{d}t}$ is the adsorption rate.

Application of REM gives rise to the change in Gibbs free energy of liquid and solid (ΔG_{V}) and diffusion activation energy (ΔG_{d}) [25], as shown in Eq. (2). In this paper, REM can reduce ΔG_{V} and ΔG_{d} due to the forced convection breaking columnar crystal. Both ΔG_{V} and ΔG_{d} can increase I by 98 % compared with that without REM. Application of nanoparticles generates the change in number of crystals with critical size (N_n^0), as shown in Eq. (3). In this paper, I value of nanoparticles increases by 50 % compared with that without nanoparticles. All those changes promote heterogeneous nucleation to refine the solidification structure. So the solidification structure of Cu–36 wt% Zn alloy can be refined by REM coupling Al_2O_3 nanoparticles due to promoting heterogeneous nucleation.

According to the analysis and experimental results above, a refined mechanism by REM and Al_2O_3 nanoparticles was discussed. First, the liquid was mixed with Cu–36 wt% Zn and Al_2O_3 nanoparticles in the melting furnace, and then poured into the furnace holding for about 30 min. In this way, some elements and Al_2O_3 nanoparticles were adequately mixed. Meanwhile, a small thermal undercooling was generated in the graphite inner mold by the cool water, leading to the formation of a thin solidified shell. Furthermore, the skin effect was induced by REM from this solid surface to the inner liquid [26]. The filmy

shell and nanoparticles provided an appropriate substrate for the heterogeneous nucleation. So the atomic clusters locating near the thin solidified shell had more opportunities to agglomerate into the stable nucleus by colliding with each other under the action of the REM coupling nanoparticles. At the same time, the Lorenz force ($F = J \times B$, where F is the Lorenz force, J is the induced current density, and B is the intensity of magnetization) resulted from the stirrer system produced continuous stirring to the solid–liquid structure. Similar fluctuation induced by the high-frequency electromagnetic field has been observed with the laser level sensor on the liquid gallium surface [27].

In the experiments, Lorenz force breaks up the thin solidified shell and makes the nuclei dissociate from the surface, at the same time making Al_2O_3 nanoparticles mix adequately. Subsequently, under the action of Lorenz force, a large number of growing nuclei move down the undercooled molten metals. As a result, they grow into equiaxed crystals and prevent the primary columnar crystal from growing into coarse columnar crystal. Finally, fine equiaxed solidification structures are completed. Figure 3 presents SEM images of the interior area of matrix alloy with nanoparticles coupling REM. Figure 3a shows that the size of Al_2O_3 nanoparticles is about 46 nm in the alloy. Figure 3b shows atomic ratio of O:Al is 2.15:1.00, which is near 1.5:1.0 for Al_2O_3. These can give a proof that Al_2O_3 nanoparticles can improve the nucleation rate with a heterogeneous nucleation core.

3.2 Mechanical performances

By adding Al_2O_3 nanoparticles and stirring, the tensile strength (average 429.28 MPa) is the strongest in all samples. The tensile strength increases by 12.85 %, 20.58 % compared with that without nanoparticles but with stirring, without nanoparticles and stirring, respectively. Meanwhile, the percentage elongation after fracture becomes the largest as the grain size becomes the finest. Figure 4 shows the percentage elongation after fracture ($A_{11.3}$) for the three specimens. It shows that by adding Al_2O_3 nanoparticles and stirring, $A_{11.3}$ (average 22.16 %) increases by 14.11 %, 19.40 % compared with that without Al_2O_3 nanoparticles but with stirring, without stirring and Al_2O_3 nanoparticles, respectively. So $A_{11.3}$ of Cu–36 wt% Zn alloy is enhanced by Al_2O_3 nanoparticles.

3.3 Dezincification corrosion resistance

Figure 5a shows the depth of dezincification layer for casting billet. It shows that Cu–36 wt% Zn with Al_2O_3 nanoparticles and stirring has the lowest depth of dezincification layer (average 66 μm) in all samples. The depth of dezincification layer decreases by 44.07 %, 78.71 % compared with that without nanoparticles but with stirring, without nanoparticles and stirring, respectively. In order to explore the mechanism, passivated layer and curves of potentiodynamic polarization were studied as below. EDS result shows that a passivation layer (Cu–Al_2O_3–Zn) may be completed to enhance the dezincification corrosion, as shown in Fig. 3a, b. Figure 5b shows measured depth of dezincification layer with Al_2O_3 nanoparticles coupling stirring.

Figure 6 shows the curves of potentiodynamic polarization which were measured for three times. The corrosion potential (E_{corr}) of matrix alloy without stirring and nanoparticles, with stirring but without nanoparticles, and the Cu–36 wt% Zn alloy by adding Al_2O_3 nanoparticles are −187.2, −177.1, and −165.0 mV (vs. SCE), respectively. Furthermore, the corrosion current densities (I_{corr}) of matrix alloy without stirring and nanoparticles, with stirring but without nanoparticles, and adding Al_2O_3 nanoparticles are −6.6587, −6.5044, and −6.7186 A·cm^{-2}, respectively. E_{corr} of alloy by adding Al_2O_3 nanoparticles (−165.0 mV) is the highest in all samples, and I_{corr} of alloy by adding Al_2O_3 nanoparticles (−6.7186 A·cm^{-2}) is the lowest in all samples. These prove that by adding Al_2O_3 nanoparticles, the

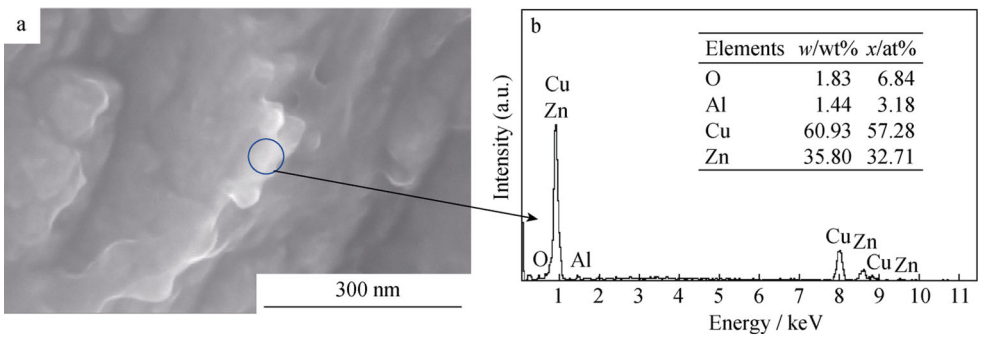

Fig. 3 SEM image **a** and EDS spectrum **b** of Al_2O_3 nanoparticles in Cu–36 wt% Zn alloys

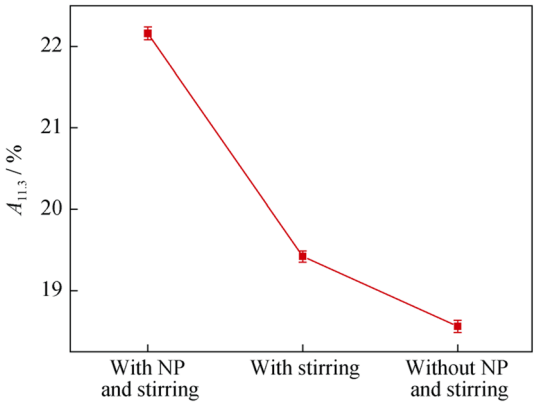

Fig. 4 Percentage elongation after fracture ($A_{11.3}$) of Cu–36 wt% Zn alloys (NP, nanoparticles)

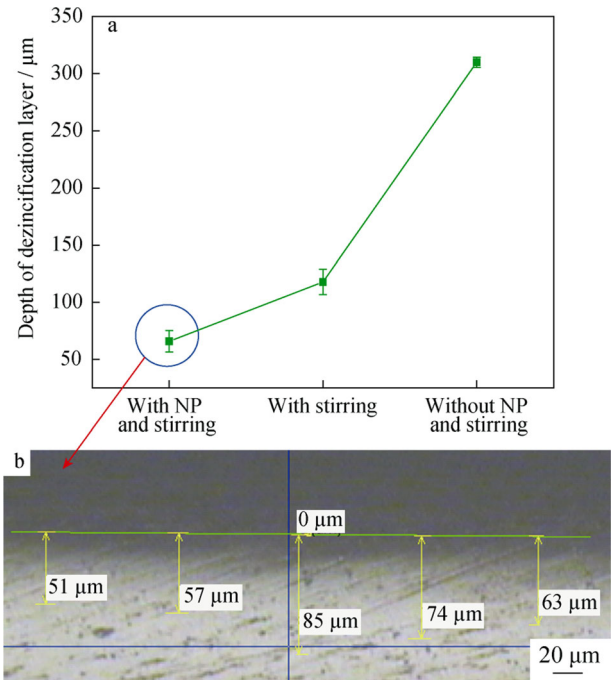

Fig. 5 Depth of dezincification layer of Cu–36 wt% Zn alloys: **a** comparison of depth and **b** OM images for depth of Cu–36 wt% Zn alloy with Al_2O_3 nanoparticles coupling REM

corrosional tendency is hindered, so the dezincification corrosion resistance is enhanced.

Meanwhile, refined grains can make quantities of the passivated layer (Cu–Al_2O_3–Zn) expand to enhance the corrosion resistance of alloy. Al_2O_3 nanoparticles in Cu–36 wt% Zn generate a compact and complete structure, and thus provide an effective protection in the 3.2 wt% NaCl solution. As a result, the dezincification corrosion resistance of Cu–36 wt% Zn alloy by adding Al_2O_3 nanoparticles is greatly improved.

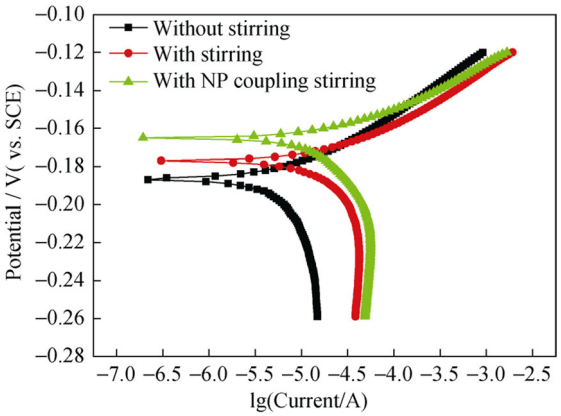

Fig. 6 Potentiodynamic polarization curves of Cu–36 wt% Zn alloys

4 Conclusion

By Al_2O_3 nanoparticles coupling stirring, Cu–36 wt% Zn alloy with refined microstructure was successfully prepared with the diameter of 16 mm. The average grain size is about 0.017 mm, which decreases by 99 % compared with that without nanoparticles and stirring. The tensile strength (R_m) and percentage elongation after fracture ($A_{11.3}$) increase by 20.58 % and 19.40 % compared with that without nanoparticles and stirring, respectively. Heterogeneous nucleation rate of nanoparticles increases by 50 % compared with that without nanoparticles. The depth of dezincification layer decreases by 78.71 % compared with that without nanoparticles and stirring, as protective layer (Cu–Al_2O_3–Zn) is formed around the grain boundaries.

Acknowledgments This study was financially supported by the National Natural Science Foundation of China (No. 51571160), the Fundamental Research Fund for Taizhou Science and Technology (No. 131KY02), the Public Welfare Projects of Science and Technology Department of Zhejiang Province (No. 2015C31143), and the Pivot Innovation Team of Shaanxi Electric Materials and Infiltration Technique (No. 15JS071).

References

[1] Wang ZJ, Zhang TL. Research and development of free-cutting nonleaded brass rod. Nonferrous Met Process. 2004;33(6):10.
[2] Kobayashi T. Strength and fracture of aluminum alloys. Mater Sci Eng. 2000;280(1):8.
[3] Zhang AS, Xu P. Refinement and metamorphism of HPb59-1 brass by trace boron. Tech Hot Work. 2005;89(7):22.
[4] Cao YQ. Application of high melting point elements Fe and Ni in casting brass. Foundry Tech. 2004;7:563.
[5] Gan FX, Guo H, Yao L. Mechanism of arsenic inhibition dezincification in brass. Chin J Corros Prot. 1991;11(1):75.
[6] Zhao HF, Dai WG, Ding JY. Effects of heat treatment on dezincification corrosion properties of C46500 brass. Shanghai Non Met. 2014;35(1):24.
[7] Han QY, Ludtka G, Zhai QJ. Materials Processing under the Influence of External Fields. New Jersey: Wiley Press; 2007. 20.

[8] Zi BT, Ba QX, Cui JZ, Xu GM. Study on axial changes of as-cast structures of Al alloy sample treated by the novel SPMF technique. Script Mater. 2000;43(3):377.
[9] Yan ZM, Li XT, Cao ZQ, Zhang XL, Li TJ. Grain refinement of horizontal continuous casting of the CuNi10Fe1Mn alloy hollow billets by rotating magnetic field (RMF). Mater Lett. 2008;62(28):4389.
[10] Ma XP, Li YJ, Yang YS. Influence of pulsed magnetic field on microstructures and macro-segregation in 2124 Al-alloy. J Mater Res. 2009;24(8):2670.
[11] Fu Y, Park J, Wang TM, Kim J, Cao ZQ, Li TJ. Modification of solidification structure under DC pulse magnetic field. J Iron Steel Res Int. 2012;S1:226.
[12] Chen Z, Wang T, Gao L, Fu H, Li T. Grain refinement and tensile properties improvement of aluminum foundry alloys by inoculation with Al-B master alloy. Mater Sci Eng A. 2012;553:32.
[13] Zhu J, Wang T, Cao F, Huang W, Fu H, Chen Z. Real time observation of equiaxed growth of Sn-Pb alloy under an applied direct current by synchrotron microradiography. Mater Lett. 2012;89:137.
[14] Brush LN, Richard N. The effect of an electric on rod-eutectic solidification in Sn–0.9 wt% Cu alloys. Mater Sci Eng A. 1997;238(1):176.
[15] Rodriguez JM, Esteva A, Meza S. A note on the control of the solidification front in the continuous casting of copper tubes. J Mate Proc Tech. 1999;96(1–3):42.
[16] Li XT, Zhao XW, Wei B, Chen FB, Yan ZM, Li TJ. Effect of rotating electromagnetic field on solidification structures and mechanical properties of tube billets of BFe10-1-1 alloy. Chin J Non Met. 2007;17(6):922.
[17] Yan Z, Liu H, Li T, Zhang X, Cao Z. Effects of alternating magnetic field and casting parameters on solidification structure and mechanical properties of copper hollow billets. Mater Des. 2009;30(4):1245.
[18] Song KX, Liu P, Tian BH. Stabilization of nano-Al_2O_3p/Cu composite after high temperature annealing treatment. Mater Sci Forum. 2005;475–479:993.
[19] Chen ML, Kang L, Yang J, Yang L, Gao H. Microstructure and mechanical properties of reinforced cast aluminum bronze by modified nano-SiC powder. Foundry. 2008;57(4):330.
[20] Flemings MC. Solidification processing. Metall Trans. 1974; 5(10):2121.
[21] Liu LZ, Ying GB, Zhu J, Lin H, Zhu CC. High-temperature compressive properties of TiC–TiB2Cu composites prepared by self-propagating high-temperature synthesis. Rare Met. 2014; 33(1):95.
[22] Kurz W, Fisher DJ. Fundamentals of Solidification. 3rd ed. Switzerland: Trans Tech Publications Ltd; 1992. 71.
[23] Chalmers B. Principles of Solidification. New York: Wiley; 1964. 6.
[24] Li J, Ma JH, Gao YL, Zhai QJ. Research on solidification structure refinement of pure aluminum by electric current pulse with parallel electrodes. Mater Sci Eng A. 2008;490(1–2):452.
[25] Zhou BL. Some non-equilibrium thermo physical problems to be studied in materials processing. Mater Sci Eng A. 2000;292(2):133.
[26] Liao X, Zhai Q, Luo J, Chen W, Gong Y. Refining mechanism of the electric current pulse on the solidification structure of pure aluminum. Acta Mater. 2007;55(9):3103.
[27] Suda M, Iwai K, Asai S. Ultra-high-strength bainitic steels. ISIJ Int. 2005;45(11):1736.